L. Garzotti, X. Garbet, A. Thyagaraja, M. R. de Baar, D. Frigione,
P. Mantica, V. Parail, B. Pégourié, L. Zabeo and JET EFDA contributors

Simulations of JET Pellet Fuelled ITB Plasmas

Simulations of JET Pellet Fuelled ITB Plasmas

L. Garzotti[1], X. Garbet[2], A. Thyagaraja[3], M. R. de Baar[4], D. Frigione[5],
P. Mantica[1], V. Parail[3], B. Pégourié[2], L. Zabeo[3]
and JET EFDA contributors*

[1]*Consorzio RFX - Associazione EURATOM-ENEA sulla Fusione, I-35127 Padova, Italy*
[2]*Association EURATOM-CEA,CEA/DSM/DRFC, CEA-Cadarache, 13108 St. Paul-lez-Durance, France*
[3]*EURATOM-UKAEA Fusion Association, Culham Science Centre, Abingdon, OX14 3DB, UK*
[4]*FOM Institute for Plasma Physics Rijnhuizen - Association Euratom-FOM, 3430 BE Nieuwegein, The Netherlands*
[5]*ENEA Centro Ricerche Frascati - Associazione Euratom-ENEA sulla fusione, 00044 Frascati (Rome), Italy*
[6]*Istituto di Fisica del Plasma EURATOM-ENEA-CNR Association, Milan, Italy*
* See annex of J. Pamela et al, "Overview of JET Results",
(Proc.20 [th] IAEA Fusion Energy Conference, Vilamoura, Portugal (2004).

ABSTRACT.

Experiments were performed on JET where high-density plasmas with an Internal Transport Barrier (ITB) were created by means of combined use of Lower Hybrid Current Drive (LHCD) and pellet injection before the barrier formation. Attempts were also made to use pellets to fuel the plasma and to sustain the density during the ITB phase. It was found that shallow pellets ablating within 15 cm from the plasma edge and far from the foot of the barrier did not destroy the ITB, whereas deeper pellets with penetration length of 30-40cm affected the barrier and led to its disappearance. Modeling of these experimental scenarios has been performed with transport and fluid turbulence codes. The codes used in the analysis were: JETTO, a 1.5 dimensional transport code, TRB, a global electrostatic fluid turbulence code and CUTIE, a global electromagnetic fluid turbulence code. The results show that for the shallow pellet case all codes reproduce the general features of the experiment, whereas for the deep pellet case, there are differences in the degree of agreement between the different codes and the experiment. Runs performed varying the pellet penetration depth indicate that not only the pellet penetration, but also the barrier strength plays a key role in the dynamics of the pellet-ITB interaction.

1. INTRODUCTION

One of the main issues about Internal Transport Barriers (ITBs) and their relevance to a reactor scenario concerns the possibility of creating and maintaining them at plasma densities close to the Greenwald limit ($n_G = I/\pi a^2$, where I and a are the plasma current and minor radius respectively).

One of the main candidates to create and fuel high-density ITB plasmas is pellet injection. The question then arises as to whether the ITB can survive the strong perturbation induced by the pellet and the fuelling of the interior of the ITB is possible without destroying the barrier itself.

To investigate this subject, experiments were performed on JET where highdensity plasmas with an Internal Transport Barrier (ITB) were created by means of the combined use of lower Hybrid Current Drive (LHCD) and pellet injection before the barrier formation. Attempts were also made to use pellets to fuel the plasma and sustain the density during the ITB phase. It was found that shallow pellets ablating within 15cm from the plasma edge and far from the foot of the barrier (located at about 50cm from the plasma edge) did not destroy the ITB, whereas faster and deeper pellets with penetration length of 30-40cm affected the barrier and led to its disappearance.

To understand the underlying physics, modeling of these experimental scenarios has been performed with transport and fluid turbulence codes. The use of different codes allows the analysis of general transport and details of the turbulence dynamics at the same time. The codes used in the analysis were: JETTO [1], a 1.5 dimensional transport code, equipped with a neutral gas and plasma shield pellet ablation model and a criterion (based on the relative values of the magnetic shear, s, and the ratio between the velocity shear and the growth rate of the Ion Temperature Gradient (ITG) modes, $\omega_{E \times B}/\gamma_{ITG}$) to describe the barrier formation, TRB [2, 3], a global electrostatic fluid turbulence code and CUTIE [4], a global electromagnetic fluid turbulence code. The three codes adopt different

approaches and, in general, have some aspects of the physic in common but differ in others. The scope of the study presented in this paper is to identify the experimental features that can be simulated by all the codes and those that can be explained only by some of them and to understand the reasons for the different results of the simulations.

In the paper the results of the simulations are presented and the physics of the interaction between the pellet and the ITB is discussed. It is found that for the shallow pellet case all codes reproduce the general features of the experiment. In particular the ITG and trapped electron turbulence level increases as a consequence of pellet injection, leading to the fast relaxation of the post-pellet density profile observed experimentally. However, for the deep pellet case, there are differences in the degree of agreement between the different codes and the experiment. In particular JETTO seems to confirm the validity of the $s-\omega_{E\times B}/\gamma_{ITG}$ criterion, TRB cannot reproduce the destruction of the ITB and CUTIE agrees qualitatively with the experiment and finds a significant reduction of the zonal flows and their shearing rate after pellet injection that is responsible for the loss of the ITB. Runs performed varying the pellet penetration depth indicate that not only the pellet penetration, but also the barrier strength plays a key role in the dynamics of the pellet-ITB interaction.

The paper is organised as follows: section 2 summarise the experimental evidence, section 3 presents the results of the simulations performed with the different codes, section 4 gives a comparative discussion of the simulations and section 5 contains the conclusions of the work.

2. EXPERIMENTAL RESULTS

To establish high-density ITB plasmas on JET [5, 6] a LHCD prelude is applied at the beginning of the discharge to set up the hollow q profile necessary for the ITB formation. LHCD is then switched off and an ohmic or low Neutral Beam Injection (NBI) power gap of about 1 s is allowed to inject pellets and increase the plasma density up to 0.7- $0.8n_G$. During this density ramp-up phase the q profile is maintained due to the slow current diffusion time. The main NBI and Ion Cyclotron Resonant Heating (ICRH) is finally applied to form the ITB and attempts were made to fuel the high performance phase with more pellets. A typical discharge is shown in figure 1, where the three phases (LHCD prelude, ohmic gap and main heating phase) can be clearly seen.

Pellets in the ohmic gap were fired from the High Field Side (HFS) launch location and pellets in the main heating phase were fired both from the Low Field Side (LFS) and Vertical High Field Side (VHFS) locations [7]. The pellet speed varied from 80 to 160m/s, the pellet mass was about $1-2\cdot10^{21}$ atoms (the reproducibility of the pellet size and the reliability of the pellet train being one of the main difficulties encountered during the experimental session) and pellet frequency was 5Hz.

To investigate the pellet-barrier interaction we chose two particular pellets from two different discharges: shot 57941 with seven shallower pellets (mass $1-2\cdot10^{21}$ atom and injection speed 80m/s) injected between 4s and 6.6s from the vertical HFS track and shot 55861 with five HFS pellets (mass $1-2\cdot10^{21}$ atom and injection speed 160m/s) injected between 4.9s and 6.9s. For shot 57941 the pellet penetration depth was about 15cm (r/a ≈ 0.85 at the injection location) whereas for

shot 55861 it was 30-40cm ($r/a \approx 0.65$ at the injection location).

As can be seen from figure 2 the barrier survives for shot 57941 and is lost after the injection of the first pellet for shot 55861. This is typical of experiments with pellet injection in ITB plasmas at JET where the barrier can survive a shallow pellet, but is always destroyed when the pellet reaches the foot of the ITB. However, in this particular case, it has to be noted that, apart from the difference in pellet penetration, the two discharges differ also because the ITB in shot 57941 is stronger than that in shot 55861.

The barrier strength is quantified by means of the ρ^*_T criterion, in use at JET to describe ITBs [8]. Essentially the quantity $\rho^*_T = \rho_s/L_T$ (where ρ_s is the ion Larmor radius at the sound speed and L_T is the temperature gradient scale length) is calculated and a barrier is said to exist where $\rho^*_T \geq 1.4 \cdot 10^{21}$. It should be noted however that this value should not be considered strictly as a threshold where a bifurcation takes place, but rather as an indication of the local steepness of the temperature profile. Regarding shot 55861, the important thing is that a discontinuity in the temperature gradient is present on the profile before pellet injection. This discontinuity is suddenly destroyed by the pellet and never reappears again. For our analysis we chose the second pellet of the main heating phase injected at 5.200 s for shot 57941 and the first pellet of the main heating phase injected at 4.935 s for shot 55861.

3. SIMULATION RESULTS

Predictive transport simulations of the selected shots have been performed with JETTO, TRB and CUTIE. The main purpose of the simulations was to reproduce the experimental features of the discharges considered and in particular those regarding the physics of the interaction between pellet and ITB. Therefore we concentrated more on the simulation of the barrier dynamics than on the exact reproduction of the plasma density and temperature profiles. Moreover, in order to establish the relative importance of pellet penetration and ITB strength in determining whether the ITB survives the pellet or not and since two discharges with same ITB strength but different pellet penetration were not available, we have simulated the injection in shot 57941 of a pellet with the same injection parameters as the one injected in shot 55861.

3.1. JETTO

Transport simulations have been performed with the JETTO code using the semiempirical mixed Bohm/gyro-Bohm transport model [9]. To visualise the density pulse better and for consistency with TRB and CUTIE simulations (see following subsections) we have performed two identical run for each shot, one with and one without pellet injection. To investigate the reaction of the barrier to the pellet injection we analysed a time interval covering the 200ms around pellet injection. This is four times longer than the simulations performed with TRB and CUTIE (50ms).

To describe pellet injection, JETTO has been equipped with a pellet injection module based on a Neutral Gas and Plasma Shield (NGPS) ablation model [10]. This module gives the pellet ablation

profile and does not take into account the possible effect of a drift of the ablated material towards the low field side of the tokamak. However, at least for this kind of shot, this phenomenon seems to be negligible [11].

To simulate the barrier formation in JETTO, the particle transport coefficient D and the ion and electron thermal diffusivities, $\chi_{i,e}$, given by the mixed Bohm/gyro-Bohm model are reduced according to a criterion which takes into account the magnetic shear s and the ratio $\omega_{E \times B}/\gamma_{ITG}$ between the shear of the E×B velocity and the growth rate of the ITG modes. Indeed, it has been observed on a statistical basis [12] that in general a barrier is formed where the condition $z = -0.14 + s - 1.47\, \omega_{E \times B}/\gamma_{ITG} < 0$ is satisfied.

Therefore the Bohm diffusion term in the mixed Bohm/gyro-Bohm transport model is multiplied by $\Theta(z)$, where Θ is the Heaviside step function. It is worth noting that the expression used in JETTO for $°ITG$ has the simplified form $\gamma_{ITG} = v_{th,i}/L_T$, where $v_{th,i}$ is the ion thermal velocity. The most important consequence of this is that the stabilising effect of the density gradient on ITG instabilities is not taken into account in the simulations performed with JETTO.

The results of the simulation for shot 57941 are shown in figures 3 and 4. To show the propagation of the density pulse and the barrier dynamics on both the ion and electron temperature profiles we plot $\delta n/n = (n_{e,pellet} - n_{e,no\ pellet})/n_{e,no\ pellet}$, $\rho^*_{Te} = \rho_s/L_{Te}$ and $\rho^*_{Ti} = \rho s/L_{Ti}$. As already said, the two latter quantities are defined in [8] and give an indication of the strength of the ITB. It can be seen from the contour plots that the density perturbation stops at the barrier where the temperature gradient remains steep, in agreement with the experimental behaviour.

The results show also that the $s - \omega_{E \times B}/\gamma_{ITG}$ criterion works for $r/a \leq 0.35$ during the whole time interval considered which corresponds to the barrier not being lost. This is illustrated in figure 4 where we plot the particle diffusion coefficient D, the plasma toroidal velocity V_T, the density gradient ∇_n and the $E \times B$ velocity shear $\omega_{E \times B}$. None of these quantities change significantly from before to after pellet injection and consequently the particle and thermal diffusivities are always suppressed for $r/a \leq 0.35$.

It is worth noting that to simulate the density decay after pellet injection the diffusion coefficient has to be increased by a factor of about 3 in the zone affected by the pellet deposition. This is consistent with simulations of other experimental scenarios made with JETTO [13]. Regarding the fuelling and the role of the different particle sources, the simulations are consistent with a picture in which the core fuelling is provided by NBI whereas pellets are responsible for the edge fuelling [11].

The situation for shot 55861 is rather different and the results are shown in figures 5 and 6. From the contour plots of $\delta n/n$, ρ^*_{Te} and ρ^*_{Ti} it can be seen that the density pulse makes its way through the barrier and the steep temperature gradient is lost after pellet injection both on the ion and electron temperature density profiles. This is again in agreement with the experiment, although it should be noted that JETTO tends to predict a somewhat weaker electron ITB than the one observed experimentally.

4

In this case it can also be seen that the diffusivity suppression is no longer effective after pellet injection. A closer look to the barrier formation criterion shows that this is due to a decrease of the $\omega_{E\times B}/\gamma_{ITG}$ term. The main causes of this are a reduction of V_T (due to the increase in the plasma mass at constant momentum input) and a flattening of ∇_n at the foot of the ITB (leading to a smaller contribution of the ∇_p term in the calculation of the radial electric field). As already pointed out the stabilising effect of ∇_n on the ITG growth rate is not taken into account in the JETTO simulations. On the other hand the s profile remains substantially unchanged, consistently with what was observed in other pellet injection experiments where, due to the slow current diffusion time, the q profile was not affected by the pellet injection [14].

As previously said, to clarify the relative role of barrier strength and pellet penetration we performed a JETTO simulation of shot 57941 but with pellet injection parameters of shot 55861. The results show that this particular barrier would also survive a relatively deeper pellet. On the other hand there is experimental evidence on JET that deep penetrating pellets lead to the disappearance of the ITB (see for example [15]); however in those cases not only the pellet penetration but also the target plasma was different from the experiments described in this paper. Therefore neither the simulations nor the experiments performed so far can provide a clear cut answer to identify the main parameter determining the ITB dynamics after pellet injection. Certainly the pellet penetration cannot be the only criterion to discriminate whether an ITB would be destroyed by pellet injection or not and more experiments featuring pellets with different penetration length injected in identical ITB plasmas are necessary to investigate this problem further.

3.2. TRB

TRB is a full torus, electrostatic, fixed flux code solving fluid equations for ITG and Trapped Electron Modes (TEM). The equations considered give the evolution of electron density and pressure, vorticity, parallel ion velocity and ion pressure. The q profile is taken from the experiment and does not evolve during the simulation. All TRB runs are carried out with 256 radial mesh points, 70 poloidal and 10 toroidal harmonics (toroidal harmonics range between 4 and 40 with a spacing of 4, i. e. n = 4, 8, 12, . . . , 40). Because of the lack of spatial resolution, the simulations were not done for the actual value of the normalised Larmor radius $\rho*$ (typically $\rho* = 5\cdot10^{-3}$ at mid-radius for B = 3T, T = 5keV, a = 1m), but for a larger value $\rho* = 10^{-3}$. The heat and particle sources were rescaled assuming a gyro-Bohm scaling.

To simulate the pellet injection a source describing the pellet ablation is switched on. The shape of the source is Gaussian. The centre and width are inferred from the interferometer profile which, in spite of the uncertainties introduced by the inversion procedure, can provide an estimate of the shape of the ablation profile. The duration of the time window during which the source is active is deduced from the duration of the H_α signal.

For shot 57941 the source was located at r/a = 0.9 which corresponds to 10cm inside the plasma and its width was estimated 0.1 r/a, corresponding to 10cm. For shot 55861 the barycentre of the

source was located at r/a = 0.7 corresponding to 30cm inside the plasma and the width was 0.25 r/a ($\approx$ 25cm). For both shots the duration is 4ms and the intensity has been kept constant and equal to $5 \cdot 10^{23}$ atom/s corresponding to a total particle inventory of $2 \cdot 10^{21}$ atoms.

The simulations carried out for both shots show the formation of strong barriers on electron and ion temperature profiles and of a weaker barrier on the density profile. This is indicated in figures 7 and 8 that, in analogy with JETTO simulations, show $\delta n/n$ and ρ^*_{Te} and ρ^*_{Ti}. It can be seen that TRB predicts the formation of two barriers, one near the plasma edge and another more internal and located at the position of minimum q. For neither shot does the density pulse cross the core ITB and a strong temperature gradient is always present on both the ion and electron channel.

Indeed, in the case of shallow pellet injection the density pulse stops before reaching the barrier and the ITB survives both on the density and the temperature profile, in agreement with the experimental observation. It is interesting to observe that in this case the strong edge localised density gradient changes the stability of the modes and induces an inward pinch at the edge. As a consequence the edge density in the shot with a pellet is lower than in the shot without.

On the other hand, for deeper pellet penetration, the density pulse reaches the barrier location and stops there. In this case, contrary to the experimental evidence, the barrier on the density profile is weakened but not completely destroyed and the barrier on the temperature profiles survives and is even amplified.

An interesting feature of TRB simulations is shown in figure 9. When the pellet is injected the intensity of the density fluctuations increases and the turbulence burst propagates inward. An enhanced turbulent activity is in agreement with the enhanced particle diffusivity needed in JETTO to model the prompt relaxation of the post-pellet profile and may explain the fast propagation of the density pulse.

3.3. CUTIE

CUTIE is a global electromagnetic fluid turbulence code. It solves the evolution equations for the fluctuating electron density, electron and ion temperature, velocity, potential and magnetic field. The pellet source is implemented exactly as in TRB. All runs are carried out on a radial mesh of 100 points and using 64 poloidal and 16 toroidal harmonics. The time-step used in CUTIE for all the simulations is 100ns, to resolve the shear Alfvén time.

In order to highlight the effect of the pellet two CUTIE runs were performed for each shot. Both runs were started from the same initial conditions and let evolve until a steady state was reached (typically 27-28 ms), then in one case a pellet was injected whereas in the other the simulations was continued without pellet injection. The main results of the simulations are shown in figures 10 and 11 where the evolution of $\delta n/n$, ρ^*_{Te} and ρ^*_{Ti} in the two runs is shown. It its clearly seen that for shot 57941 the density pulse stops at the barrier and the barrier survives, whereas for shot 55861 the barrier is weakened by the pellet and the density pulse reaches the plasma centre, in qualitative agreement with the experimental observation.

6

However some details of the simulations differ from the experimental behaviour. In particular for shot 57941 CUTIE predicts, rather than a wide ITB at r/a = 0.4 (like in shot 55861), the existence of two narrower ITBs located at the surfaces corresponding to q = 2 (r/a = 0.4) and q = 3 (r/a = 0.7). This is a consequence of the main mechanism of ITB formation in CUTIE that involves a local flattening of the q profile at resonant surfaces induced by the dynamo effect associated with electromagnetic modes and resulting in a stabilisation of ITG turbulence [16]. Indeed temperature profiles featuring a double ITB are seen on JET even in shots similar to 57941.

Another difference between CUTIE predictions and experimental evidence is that (as can be seen from figures 10 and 11) CUTIE finds after the pellet injection an increase in the ohmic power deposition and in the local temperature gradient in the region perturbed by the pellet deposition. This effect is not seen in the experiment and is due to the fact that CUTIE takes into account the increase in resistivity due to the cooling induced by the pellet but not the decrease in Z_{eff} due to the impurity dilution. In the experiment both effects are present and tend to compensate, leaving the total ohmic power deposition unchanged. It can be noted that the difference between experiment and CUTIE simulation is more evident for shot 55861 (lower density) than 57941 (higher density) because in the first case the relative cooling due to the pellet is greater.

Apart from the pellet penetration length, the main difference between the two shots concerns the structure of the zonal flows. Figures 12 and 13 show the evolution of the parameter $\rho^*_{zf} = \rho_s/L_{zf}$ for the two shots. Here L_{zf} is defined similarly to LT and represents the typical gradient scale length of the zonal flows. It can be seen that in shot 57941 the short scale gradients of the zonal flows are maintained in the barrier zone even after the pellet ablation, whereas the gradient scale length is strongly reduced in shot 55861. Therefore the CUTIE simulation would indicate that the main reason for the barrier destruction observed in association with deeper pellet injection is the reduction of the zonal flow shearing rate and the reduction of its stabilising effect on turbulence in the barrier zone.

Simulations of shot 57941 with pellet injection parameters from shot 55861 were also performed with CUTIE. The indication from this run is that the ITB is not destroyed although significant MHD activity is created near the foot of the barrier and energy confinement is lower. The density evolution shows that the pellet pulse is reflected at the ITB. The barriers in T_e and T_i steepen. The structure of the zonal flow is significantly changed outside the barrier in the pellet injection region (r/a = 0.7) but the level at the barrier remains the same as in the shallow pellet case although it moves slightly inwards. The q profile does not change significantly. This is in qualitative agreement with JETTO and indicates that a strong ITB could survive the injection of relatively deep pellets.

4. DISCUSSION

Simulations in reasonable qualitative agreement with the experiment and performed with both global transport and fluid turbulence codes permit the analysis of different aspects of the dynamics of ITB in pellet fuelled plasmas. Transport simulation performed with JETTO indicate that the

empirical criterion described in [12] and based on the relative values of the magnetic shear s—and the $\omega_{E\times B}$ drift velocity shear provides the basic physics to simulate the behaviour of the ITB. However in its present form this criterion is over-simplified and does not take in to account the stabilising effect on ITG modes of ∇n. Moreover, since this criterion is based on a statistical analysis and since JETTO is a transport code which solves diffusion equations, the detailed analysis of the dynamics of the ITB is beyond the capabilities of this tool. Nevertheless JETTO runs demonstrate the need for an increased transport in the zone perturbed by the pellet, although they are not able to identify the origin of the increased diffusivity.

Further insight can be gained with fluid turbulence codes like TRB and CUTIE. In particular, TRB is able to explain the increased diffusivity and to relate it to an enhanced level of density fluctuations caused by turbulence induced by TEM and ITG modes. Moreover it simulates the stopping of the density pulse at the foot of the barrier. However TRB is not able to reproduce the different response of the ITB to shallow and deeper pellets and exhibits the formation of strong ITBs surviving pellet injection in both cases.

An even more detailed understanding of the phenomenology is obtained with CUTIE. The dynamics of the zonal flows is the main difference demonstrated by CUTIE between the shallow and the deep injection case. In fact, after pellet injection, zonal flows in the ITB region are significantly damped and their shearing rate is significantly reduced for the deep pellet case. This can account for the disappearance of the ITB.

The main reason for the different results obtained with TRB and CUTIE is probably the different mechanisms that govern the ITB formation in the two codes. In TRB when a q profile with a minimum is prescribed an ITB appears at the qmin location. This is a consequence of the stabilisation effect induced by the increased distance between

resonant surfaces near qmin. Since the q profile is kept fixed during the simulation, once an ITB is formed it tends to be very robust and it is difficult to destroy it. On the other hand, as we already pointed out, the main mechanism of ITB formation in CUTIE involves a local flattening of the q profile at resonant surfaces induced by the dynamo effect associated with electromagnetic modes and resulting in a stabilisation of ITG turbulence. Since in CUTIE q is evolved self-consistently with the other plasma parameters, the whole ITB dynamics is richer and it is easier for the ITB to disappear after being triggered, for example when the cooling associated with pellet injection increases the plasma resistivity and therefore tends to decrease the efficiency of the dynamo. Indeed, another important difference between TRB and CUTIE is the way the two codes treat collisionality, which is fixed in TRB and calculated self-consistently with the rest of the plasma parameters in CUTIE.

Runs performed with the different codes and modifying the pellet injection parameters and penetration depth indicate that not only the pellet penetration but also the ITB strength should be taken into consideration to establish whether a particular transport barrier can survive pellet injection or not. In order to further investigate and clarify this point one would need more experiments with injection of different pellets into substantially identical ITB, which have not been performed yet.

CONCLUSIONS

Experiments have been done at JET to fuel high density ITB plasmas by means of pellet injection. It is seen experimentally that shallow pellets maintain the ITB but do not fuel the plasma core and deeper pellets produce a density pulse that reaches the plasma centre but destroys the ITB.

Different simulation approaches have been attempted to analyse the dynamics of ITBs when pellet injection is performed. A transport code (JETTO) and two fluid turbulence codes (TRB and CUTIE) have been used. For the shallow pellet case all codes reproduce the general features of the experiment. In particular it is found that the ITG and trapped electron turbulence level increases as a consequence of pellet injection, leading to the fast relaxation of the post-pellet density profile observed experimentally. JETTO simulations also indicate that the beam particle source is responsible for the core fuelling whereas pellets provide the particle source at the plasma edge in agreement with the experimental observations.

For the deep pellet case, there are differences in the degree of agreement between the different codes and the experiment. In particular JETTO seems to confirm the validity of the s—" !E°—B/ °ITG criterion. TRB simulates well the increased turbulence and associated diffusivity following pellet injection, but it is not able to reproduce the destruction of the ITB observed in the case of deeper pellet injection. CUTIE simulates reasonably well most of the experimental features. In particular it shows that the reduction of the zonal flow shearing rate after pellet injection can explain the different reaction of the barrier to the pellet deposition profile and the loss of the ITB when pellet injection is too deep or the barrier is not strong enough.

REFERENCES

[1].   G. Cenacchi and A. Taroni, JETTO: A free-boundary plasma transport code (basic version), Report JET-IR(88)03, JET Joint Undertaking, Joint European Torus (1988)

[2].   X. Garbet, C. Bourdelle, G. T. Hoang, P. Maget, S. Benkadda, P. Beyer, C. Figarella, I. Voitsekovitch, O. Agullo and N. Bian, Phys. Plasmas **8** (2001) 2793

[3].   X. Garbet, et al., Plasma Phys. Control. Fusion **46** (2004) B557

[4].   A. Thyagaraja, P. J. Knight and N. Loureiro, Eur. J. Mech. B/Fluids **23** (2004) 475

[5].   D. Frigione, C. Challis, M. de Baar, C. Bourdelle, F. Crisanti, R. de Angelis, P. de Vries, B. Esposito, L. Garzotti, E. Giovannozzi, N. Hawkes and EFDA-JET contributors, in Proc. 30th EPS Conference on Contr. Fusion and Plasma Phys., St. Petersburg 2003, ECA Vol. 27A, P-2.91

[6].   C. Challis, Plasma Phys. Control. Fusion **46** (2004) B23

[7].   A. Géraud, L. Garzotti, P. T. Lang, A. Lorenz, B. Pégourié, G.L. Schmidt, B. Alper, T. T. C. Jones, P. Monier-Garbet, J. Strachan, M. Stamp, P. Bennett, J.L. Maréchal, R. Mooney, J. Ongena, M. J. Watson, D. J. Wilson and JET-EFDA contributors, in Proc. 30th EPS Conference on Contr. Fusion and Plasma Phys., St. Petersburg 2003, ECA Vol. 27A, P-1.97

[8].   G. Tresset, X. Litaudon, D. Moreau, X. Garbet and Contributors to the EFDA-JET Work Programme, Nucl. Fusion **42** (2002) 520

[9]. M. Erba, A. Cherubini, V. V. Parail, E. Springmann and A. Taroni, Plasma Phys. Control. Fusion **39** (1997) 261

[10]. L. Garzotti, B. Pégourié, A. Géraud, D. Frigione and L. R. Baylor, Nucl. Fusion 37 (1997) 1167

[11]. L. Garzotti, C. Challis, M. de Baar, D. Frigione, G. Corrigan, X. Garbet, P. Mantica, V. Parail, B. Pégourié, L. Zabeo and contributors to the EFDA-JET work programme, in Proc. 30th EPS Conference on Contr. Fusion and Plasma Phys., St. Petersburg 2003, ECA Vol. 27A, P-2.92

[12]. T. J. J. Tala, J. A. Heikkinen, V. V. Parail, Yu. F. Baranov and S. J. Karttunen, Plasma Phys. Control. Fusion 43 (2001) 507

[13]. L. Garzotti, X. Garbet, P. Mantica, V. Parail, M. Valovic, G. Corrigan, D. Heading, T.T.C. Jones, P. Lang, H. Nordman, B. Pégourié, G. Saibene, J. Spence, P. Strand, J. Weiland and contributors to the EFDA-JET Workprogramme, Nucl. Fusion **43** (2003) 1829

[14]. P. T. Lang, B. Alper, L. R. Baylor, M. Beurskens, J. G. Cordey, R. Dux, R. Felton, L. Garzotti, G. Haas, L. D. Horton, S. Jachmich, T. T. C. Jones, P. J. Lomas, A. Lorenz, M. Maraschek, H. W. Müller, J. Ongena, J. Rapp, M. Reich, K. F. Renk, R. Sartori, G. Schmidt, M. Stamp, W. Suttrop, E. Villedieu and EFDA-JET Work Programme Collaborators, Nucl. Fusion **42** (2002) 388

[15]. P. Mantica, G. Gorini, F. Imbeaux, J. Kinsey, Y. Sarazin, R. Budny, I. Coffey, R. Dux, X. Garbet, L. Garzotti, C. Ingesson, M. Kissick, V. Parail, C. Sozzi, A. Walden and contributors to the EFDA-JET Workprogramme, Plasma Phys. Control. Fusion **44** (2002) 2185

[16]. M. R. De Baar, A. Thyagaraja, G. M. D. Hogeweij, P. J. Knight and E. Min, Phys. Rev. Lett. 94 (2005) 035002
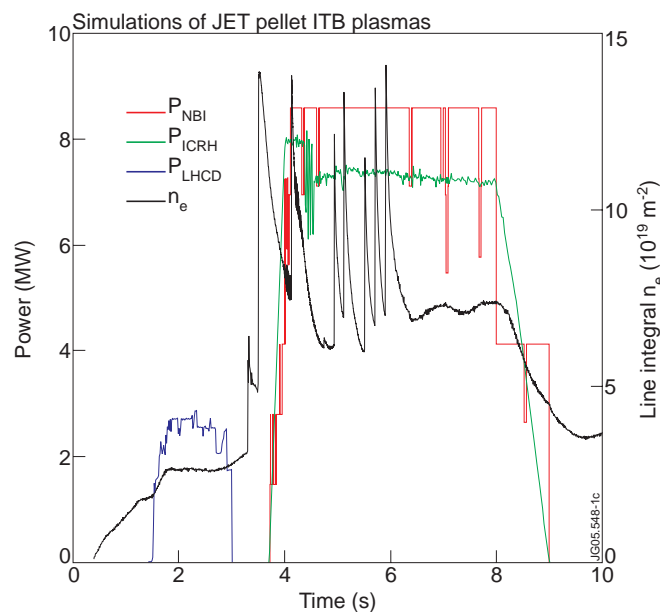
Figure 1: Typical waveforms for the experiments on pellet fuelling of high density ITBs described in the paper (shot 55861). The three phases are visible: LHCD prelude (1.5s-3s), ohmic gap (3s-4s) and main heating phase (4s-9s).
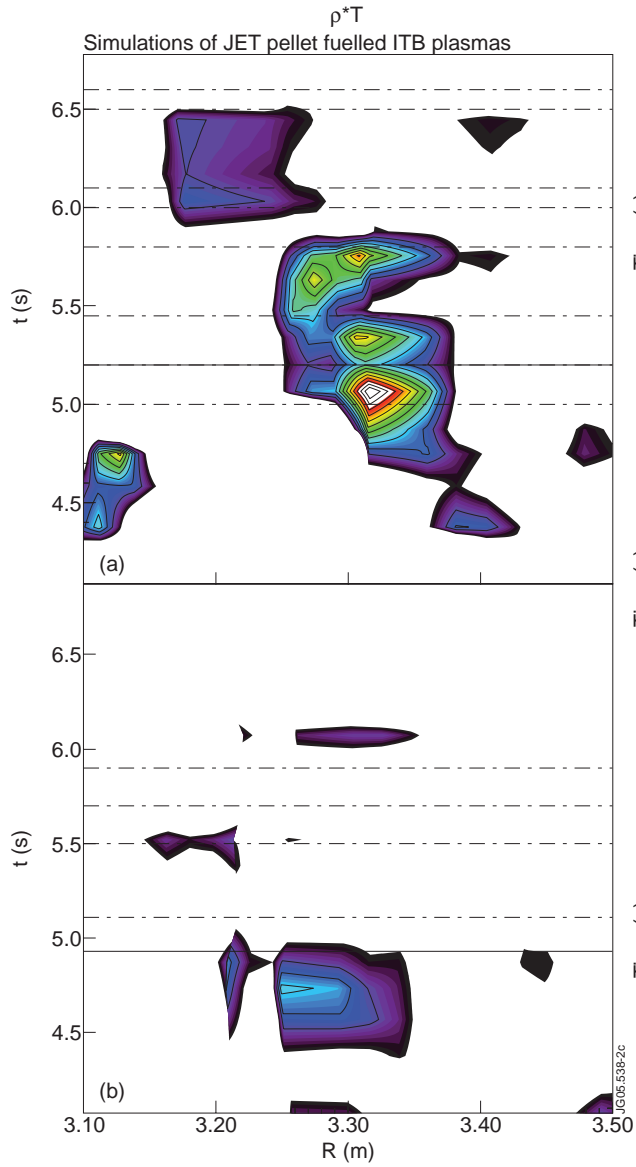
10

Figure 2: ρ_T^* for Pulse No's: 57941 (a) and 55861 (b). Electron temperature is considered in this case. The horizontal lines mark pellet injection. The two solid lines indicate the pellets considered for the simulations presented in the paper.
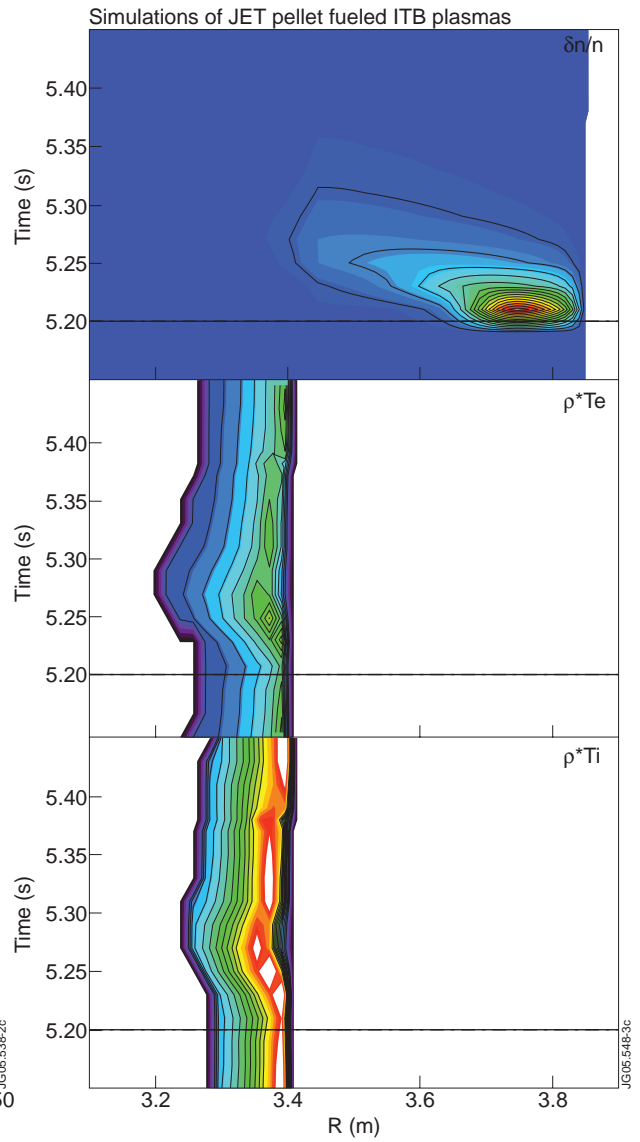
Figure 3: $\delta n/n$, ρ_{Te}^* and ρ_{Ti}^* from JETTO simulation for Pulse No: 57941. The scale for the $\delta n/n$ contours is arbitrary.
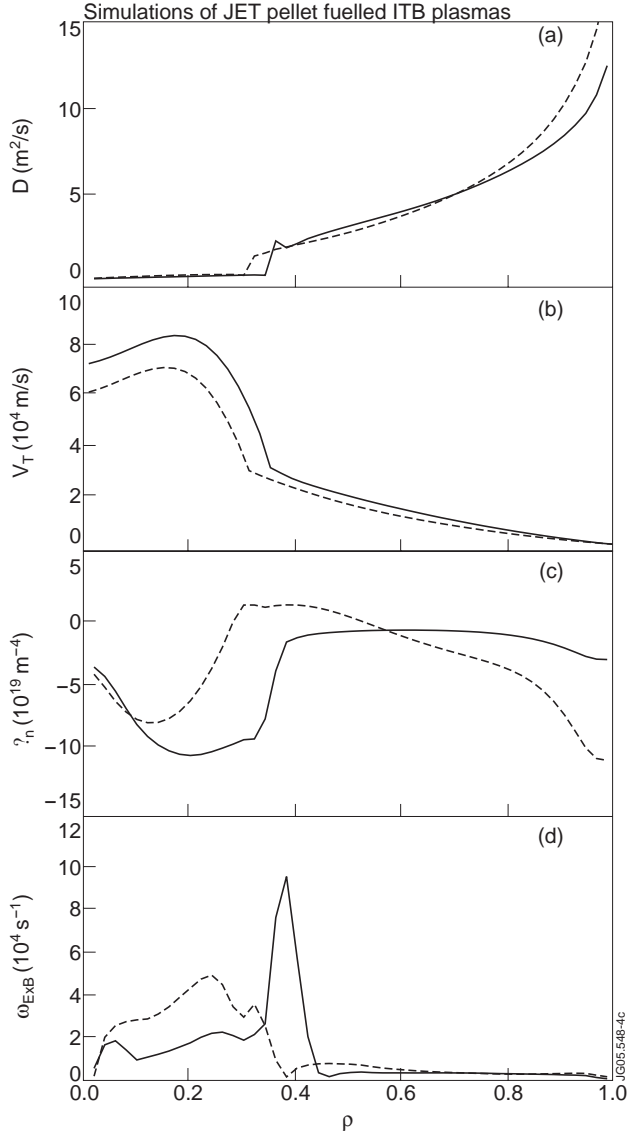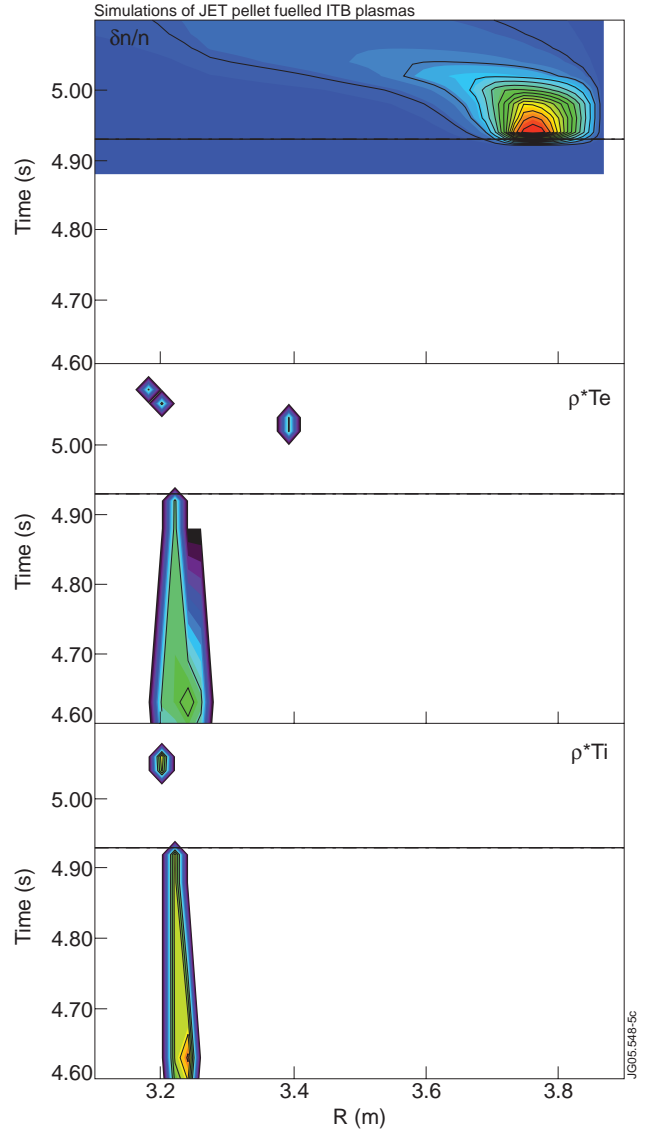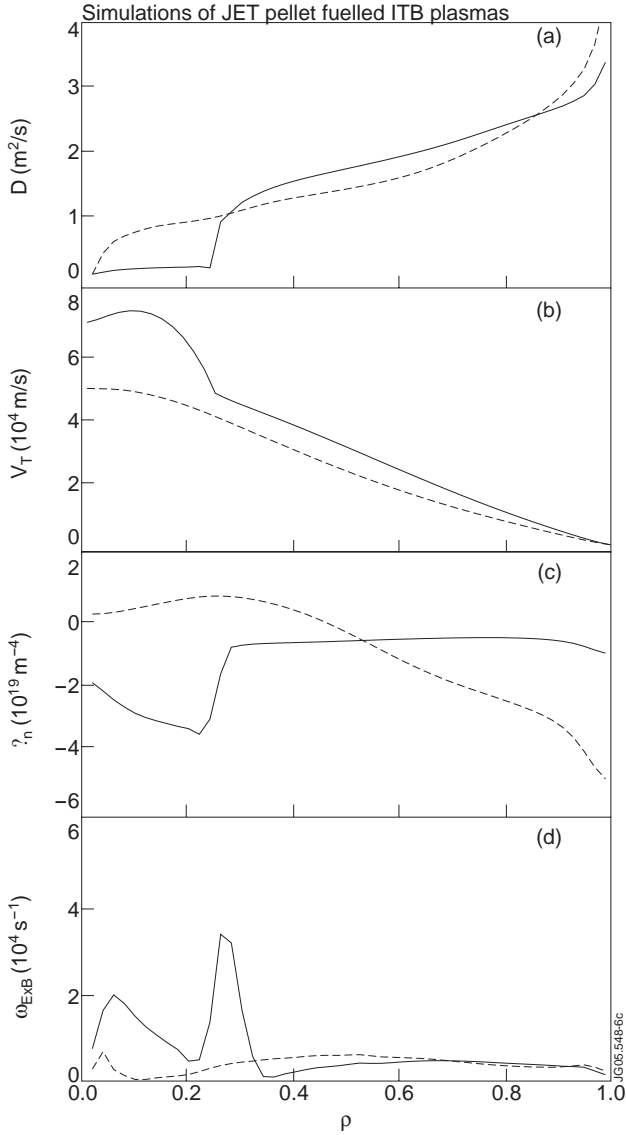
Figure 4: JETTO simulation for JET Pulse No: 57941 (the pellet is injected at t=5.2s and does not destroy the ITB). The solid lines are the pre-pellet profiles (t=5.19s), whereas the dashed lines are the post-pellet profiles (t=5.24s). The plot shows: a) particle diffusion coefficient, b) plasma toroidal rotation velocity, c) density gradient and d) $\omega_{E\times B}$ shear. The profiles before and after pellet injection remain similar. The suppression of D according to the $s - \omega_{E\times B}/\gamma_{ITG}$ criterion indicates that the ITB is not destroyed.

Figure 5: $\delta n/n$, ρ_{Te}^* and ρ_{Ti}^* from JETTO simulation for Pulse No: 55861. The scale for the $\delta n/n$ contours is arbitrary.

Figure 6: JETTO simulation for JET Pulse No: 55861 (the pellet is injected at t=4.935s and destroys the ITB). The solid lines are the pre-pellet profiles (t=4.92s), whereas the dashed lines are the post-pellet profiles (t=5.06s). The plot shows: a) particle diffusion coefficient, b) plasma toroidal rotation velocity, c) density gradient and d) $\omega_{E\times B}$ shear. D is reduced according to the $s - \omega_{E\times B}/\gamma_{ITG}$ criterion before pellet injection but not after, indicating that the pellet destroys the ITB.
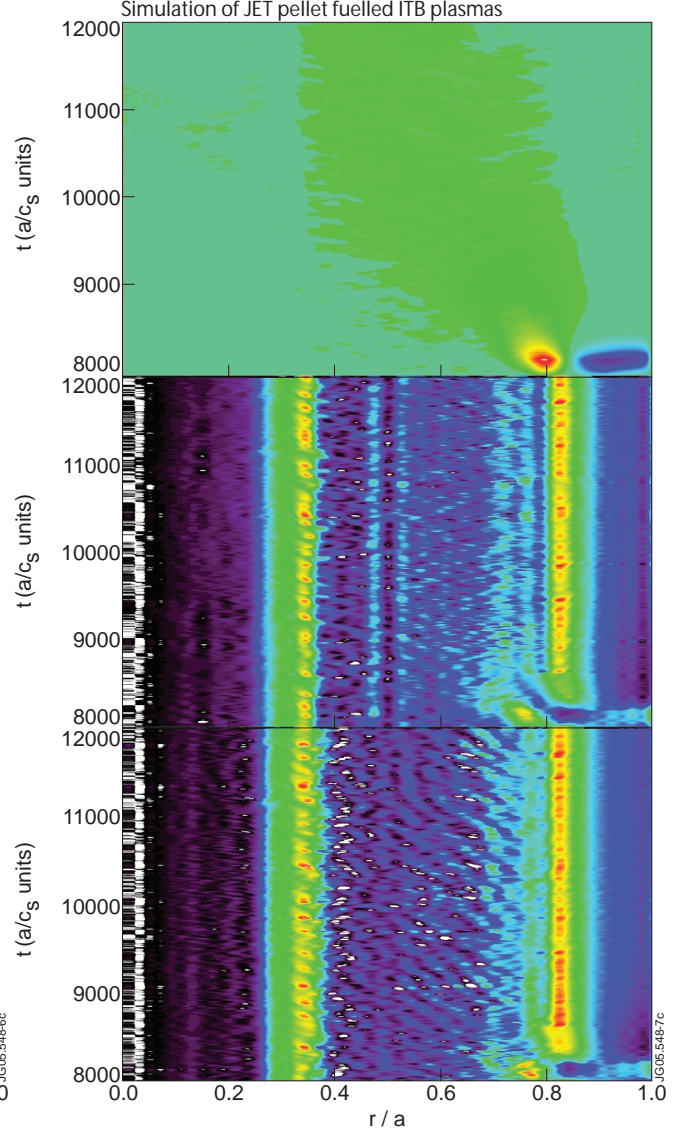
Figure 7: Same as figure 3 for TRB simulation of shot 57941 (top: $\delta n/n$, centre: $\rho_{Te}*$ and bottom: $\rho_{Ti}*$). The time is in units of a/cs where a is the plasma minor radius and c_s is the sound speed at half radius. The link with the physical time, however, is not simple because the simulations were done for an effectively smaller machine with particle and heat sources rescaled from JET data assuming a gyro-Bohm scaling law. The actual time step a/c_s is calculated by comparing the experimental confinement time in JET to the value calculated by the TRB code. For reference the total length of the run was of the order of 27.6ms and the pellet ablation source was switched on at the beginning of the simulation (t = 8000a/c_s) and lasted 4ms.
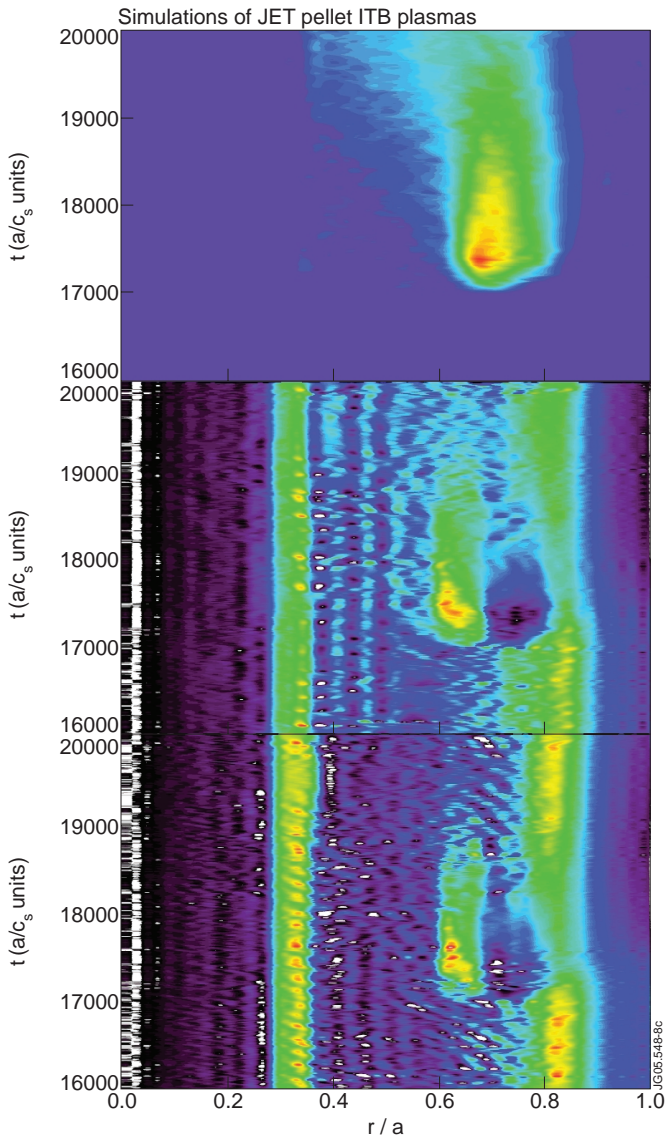
13

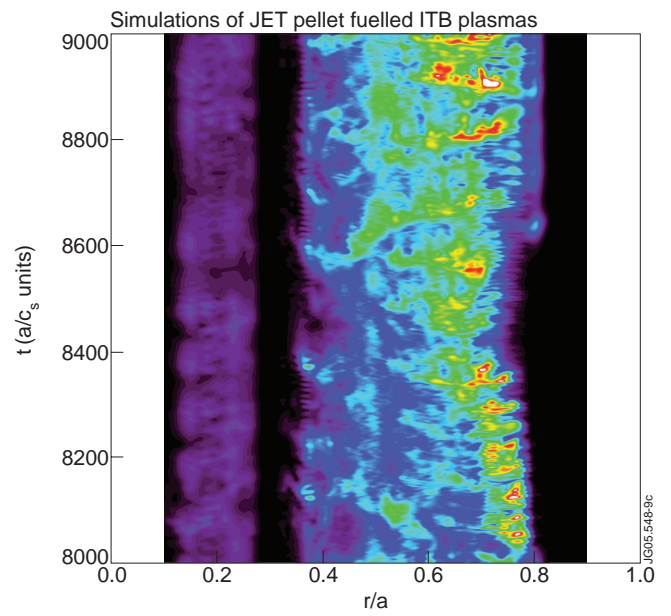*Figure 8: Same as figure 5 for TRB simulation of shot 55861 (top: $\delta n/n$, centre: $\rho_{Te}*$ and bottom: $\rho_{Ti}*$).*

Figure 9: Propagation of enhanced density fluctuations $\tilde{n}/<n_i>$ for Pulse No: 57941 (shallow pellet) given by TRB. $\tilde{n}$ and $<n_i>$ are the fluctuating and average part of the density profile respectively.
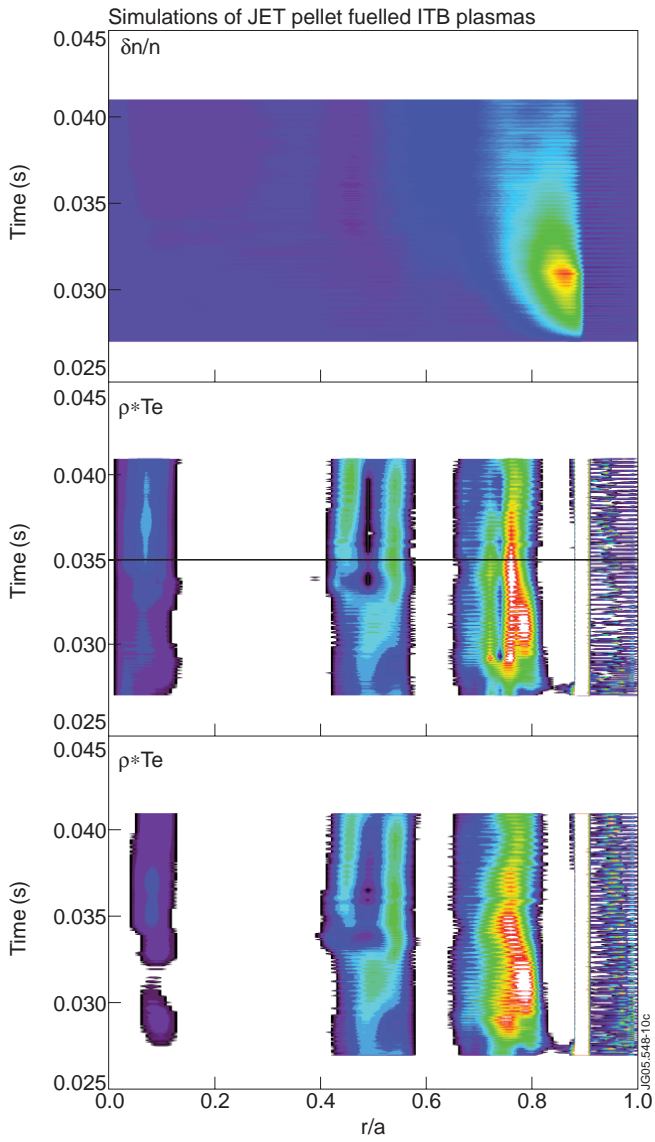
Figure 10. Same as figure 3 for CUTIE simulation of Pulse No: 57941 (shallow pellet). The data are shown starting from the pellet injection at t = 27ms.
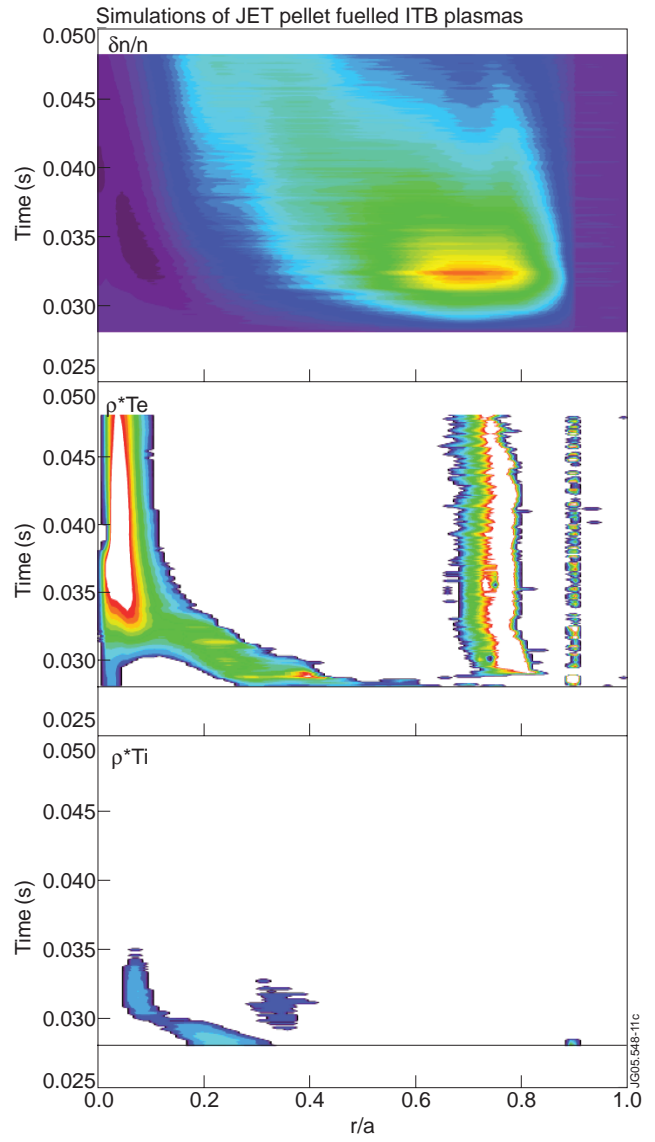
Figure 11. Same as figure 3 for CUTIE simulation of Pulse No: 55861 (deep pellet). Also in this case the data are shown starting from the pellet injection at t = 28ms. Before this time the simulations develops an ITB at r/a = 0.4.
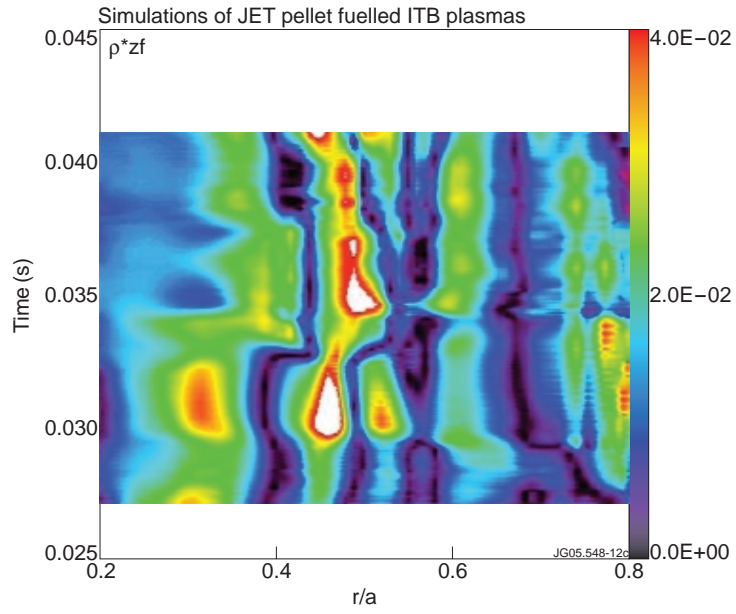
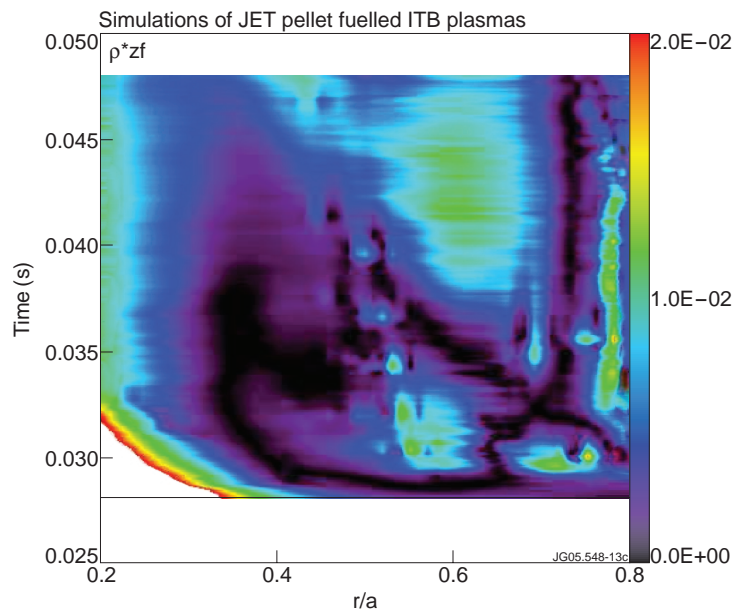*Figure 12. Space time evolution of the zonal flow gradient from CUTIE simulation of Pulse No: 57941.*

Figure 13. Space time evolution of the zonal flow gradient from CUTIE simulation of Pulse No: 55861.